Comparison of Digital Signal Processing Approaches for Subcarrier Multiplexed 5G and Beyond Analog Fronthaul

Shabnam Noor[1,*], Philippos Assimakopoulos[1], Minqi Wang[2], Hazim A. Abdulsada[1], Naveena Genay[2], Luiz Anet Neto[2], Philippe Chanclou[2] and Nathan J. Gomes[1]

[1] *Communications Research Group, University of Kent, Canterbury, UK*
[2] *Access Networks Group, Orange Labs, Lannion, France*
**Corresponding author: S.Noor@kent.ac.uk*

Received 22 October 2019

Analog fronthaul transport architectures with digital signal processing at the end stations are promising as they have the potential to achieve high spectral efficiencies, increased flexibility and reduced latency. In this paper, two digital techniques for frequency domain multiplexing/de-multiplexing large numbers of channels are contrasted: one operates on the pre-Inverse Fast Fourier Transform (IFFT) "frequency-domain" samples while the other does so on the post-IFFT "time-domain" samples. Performance criteria including computational complexity and sampling rate requirements are used in the comparison. Following modeling and simulation of the techniques, implemented within a radio-over-fiber transport architecture, error vector magnitude performance estimates are obtained. These results show that each technique has performance advantages under specific channel transport scenarios.

1. INTRODUCTION

Digital transport techniques in the fronthaul section of the Radio Access Network (RAN), traditionally based on the transportation of digitized radio samples [1], cannot scale to the signal bandwidths employed by the 5th generation (5G) mobile network [2], [3]. Furthermore, the use of multiple antenna techniques such as massive Multiple-Input Multiple-Output (mMIMO) means that bit rates over the fronthaul not only scale with the number of radio access technologies, signal bandwidths, carriers and sectors but also with the number of (spatial) radio streams, making the use of such transport techniques exceptionally challenging [2-8].

A concept diagram of a next-generation mobile network is shown in Fig. 1. The Core Network (CN) is connected through the backhaul to a Central Unit (CU) where some higher-layer RAN protocols are executed. The 3GPP has standardized the F1 interface between the CU and a Distributed Unit (DU), which connects the packet data convergence protocol (PDCP) to the radio link control (RLC) layers of the mobile stack [7], [8]. This transport network section is often termed the mid-haul. The remaining RAN protocol stack processing is split between the DU and a Radio Unit (RU). 3GPP has not reached a consensus on the split point in RAN functions between the DU and RU, but possible options within the baseband Physical (PHY) layer have been proposed [4-10]. The fronthaul is the transport network for this F2 interface between the functionally decomposed DU and RU.

As stated, an important aspect for 5G and beyond systems will be the increasing use of MIMO and, specifically, mMIMO antenna systems, as portrayed by the active antenna unit (AAU) in Fig.1, The complexity of handling within the AAU, and transporting to it, signals for each antenna element [8], [9], means, that current arrays are partitioned into sub-arrays, with a requirement to transport a pre-coded signal for each subarray, only. Thus, hybrid beamforming is used with some analog phase/amplitude control creating the different possible beam directions for each sub-array. A fronthaul for such an AAU needs to transport different streams for the sub-arrays, referred to as layers, plus some control signals for amplitude and phase weights. With the new DU-RU digital functional splits, with 5G bandwidths up to 400 MHz and eight layers, bit-rate requirements are expected to be between 16 Gbps and hundreds of Gbps, as the selected split point varies from the top to the bottom of the RAN PHY layer [9]. Both bandwidth and number of layers are expected to increase in the future. Furthermore, functional splitting can impede the use of distributed MIMO techniques due to increased fronthaul latency and latency variations (packet jitter) as the split point between DU and RU is moved higher within the Physical (PHY) layer, meaning that splits that can provide the highest data rate reductions are also the most latency

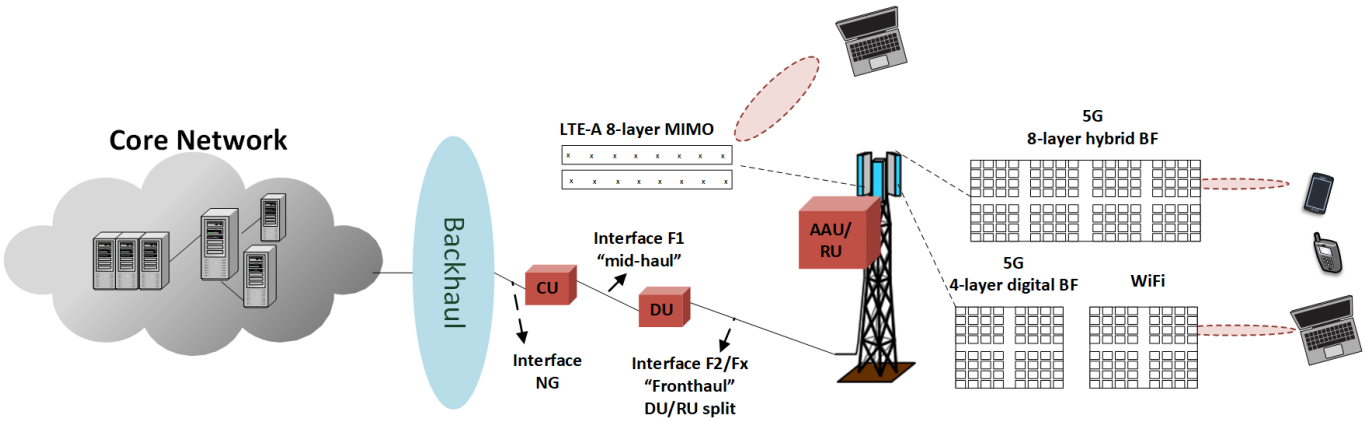

Fig. 1. A high-level functional description of the end-to-end 5G (and beyond) network, focusing more on the edge of the network (mid-haul and fronthaul).

constrained for distributed MIMO processing operations [5], [6].

Compared to digital transport, analog transport, although susceptible to impairments of distortion and additive noise from RF and optical components, achieves higher spectral efficiencies and alleviates the latency constraints [9], [11-23]. Analog transport is also capable natively of supporting multiple RAN technologies from different vendors, and for different mobile operators, without interoperability issues, sharing antennas and a single fiber infrastructure (as used in Distributed Antenna Systems) [11], [12]. Thus, analog transport has gained renewed interest for the fronthaul of the 5G (and beyond) RAN [9], [16-24]. Analog Radio-over-Fiber (RoF) can transport multiplexes of the radio signals' bandwidths, using their different carrier frequencies, or through translation to different intermediate frequencies (necessary for MIMO, when the radio signals are at the same frequency), by Subcarrier Multiplexing (SCM). Systems employing microwave/RF up-/down-converters, amplifiers, filters, splitters/combiners, etc., have traditionally been used by neutral host providers with propriety equipment under bespoke, scenario-dependent setup conditions [11], [12], [15], [17]. This lacks deployment flexibility and adaptability. The 5G and beyond RAN will need to be flexible and scalable, able to meet differing requirements across a wide range of use cases such as AR/VR, gaming and immersive applications for Industry 4.0 [8], [25]. Part of these requirements emanates from the need to accommodate variable 5G bandwidths, latencies and numerologies[1]. Furthermore, a system may include not only different Long-Term Evolution (LTE) and 5G numerologies but also those employed by Wireless Local Area Networks (WLANs) in a Heterogeneous Network (HetNet) deployment.

Such flexibility/adaptability is possible in an analog fronthaul that employs key Digital Signal Processing (DSP) techniques for the multiplexing/aggregation and de-multiplexing/de-aggregation of channels [19-24]. A DSP-assisted analog fronthaul that is inherently flexible, able to scale to different bandwidths, numerologies and modulation formats, was described in [22]. Furthermore, it was shown how such a system could be used with arbitrarily low sampling rates and analog bandwidth at the receiving end (i.e. at the RU) by the introduction of limited analog processing. Thus, the focus in [22] was on the receiver side processing and on the proposed mapping technique allowing a simplification of receiver side processing.

[1] Numerologies are the different specified numbers and spacings of the subcarriers in the Orthogonal Frequency Division Multiplexed (OFDM) signal waveforms employed.

However, a detailed analysis and performance comparison between different DSP-assisted FDM approaches is currently missing from the available literature. Such an analysis is of prime importance due to the challenges facing digital transport fronthaul links with current and future mobile network generations. In this paper, we specifically analyze two main techniques, both performing Frequency-Domain Multiplexing (FDM) that leads to SCM over the analog RoF link. The first operates on time-domain samples, while the second operates on frequency-domain samples. The latter is based on the multiplexing technique presented in [22] but this is the only similarity between the DSP-assisted approach in [22] and the techniques presented here. The focus in this paper is on the processing elements of the two FDM techniques and their effect on overall system complexity and performance. The computational complexity, sampling rates, processing latencies and analog performance in terms of error vector magnitude (EVM) are considered to fully understand the relative advantages and disadvantages of each approach.

The paper is organized as follows: Section 2 provides an overview of the two techniques and how they fit within a next-generation mobile network architecture. This is followed by an analysis of their complexity considering computations and sampling rates in Section 3. In Section 4, EVM performance estimates for back-to-back and simulated and experimental optical links are presented to compare performance. Section 5 presents the main conclusions.

2. DSP-ASSISTED SCM ARCHITECTURE

A conceptual view of the proposed DSP-assisted SCM architecture is shown in Fig. 2. At the DU, digital samples of each stream are mapped into their channels and the channels are digitally multiplexed to form a composite FDM signal. After digital-to-analog conversion this is used to modulate an optical transmitter creating the SCM analog RoF transport. At the receiving end (the RU) there may be some analog processing, analog-to-digital conversion, and digital processing to recover the digital samples of the transported streams.

Two types of processing technique for channel multiplexing can be used, as shown in more detail in Fig. 3: the first multiplexes channels using the frequency-domain samples, and employs a single-IFFT operation to convert the frequency domain multiplex into a time domain waveform; the second employs Digital Up-Converters (DUCs) and a summer to combine a number of IFFT outputs (with each IFFT outputting a single time-domain channel) into a composite multiplex. Both techniques create a frequency-domain multiplex. For the remainder of the paper the former technique will be termed the

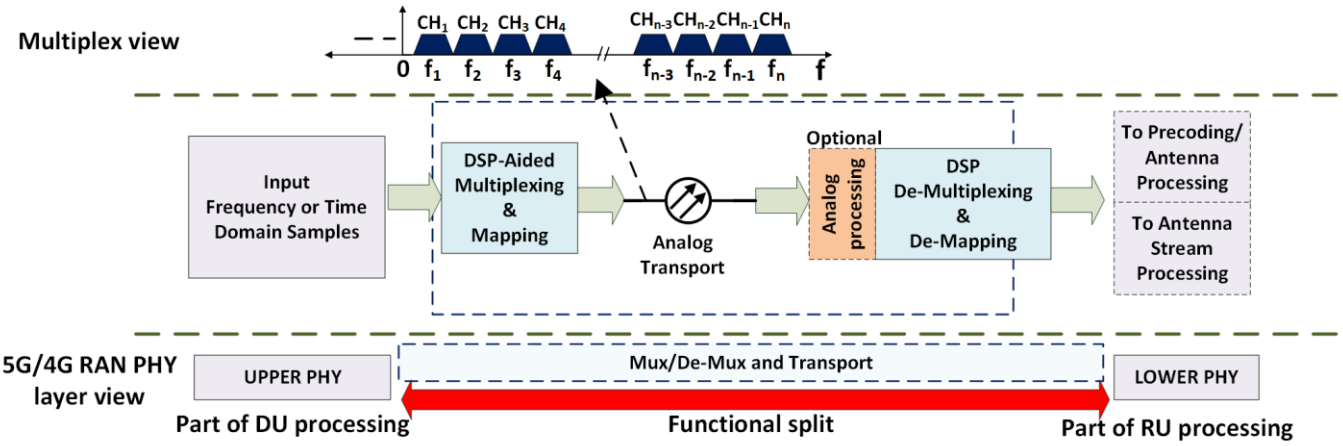

Fig. 2. Conceptual view of the proposed DSP-assisted SCM architecture and DU and RU processes. The DSP-aided multiplexing part is further elaborated in Fig. 3 and the de-multiplexing in Fig. 4. DSP, Digital Signal Processing; CH, Channel; PHY, Physical Layer (LTE/5G RAN).

frequency-domain samples-based technique, while the latter will be termed the time-domain samples technique. Also, the term "single-IFFT operation" is used for the frequency-domain samples technique (implying that only a single IFFT is used to convert the multiplex into the time-domain). Note that both techniques are inherently flexible: The channels comprising a multiplex can have different bandwidths and/or employ different modulation schemes. Both techniques can easily adapt to changes in the RF/mmW frequencies that the transported channels need to occupy at the RU. Note that if generation of mmW signals at the RU is required, a SCM/Intermediate Frequency (IF) RoF (SCM/IF-RoF) scheme can be employed with remote local oscillator delivery through optical heterodyning (as was demonstrated in [22]) or with electrical up-conversion at the RU [21]. In either case, dispersion-related effects are minimal. While not treated in this paper, these multiplexes can also comprise different numerologies by appropriate control of sampling rates, and can comprise a mixture of single sideband (SSB) and dual sideband (with conjugate symmetry)-derived channels (for the frequency-domain samples technique, some of this flexibility was demonstrated in in [22]).

A combination of the two techniques can also be envisaged, whereby each single-IFFT process is used to multiplex several channels, but the outputs of each single-IFFT are combined to form a "super-multiplex" through their own DUCs. While this is an interesting operational regime, which could be used to aggregate groupings of channels based on mobile operators, radio access network technologies, or other relevant mobile network associations, such as network slices, it will not be treated in this paper, and is instead deferred to a future article.

Following analog transport over the fronthaul, a number of de-multiplexing approaches are possible at the RU. For a fully digital-approach, shown in Fig. 4 (a), assuming the RU has sufficient sampling rate capabilities, the received analog signal multiplexes are converted directly into the digital domain through an Analog-to-Digital Converter (ADC) (note that some wide-band filtering is usually employed prior to the ADC). Then each channel is directly down-converted to baseband through a Digital Down Converter (DDC).

Alternatively, if there are sampling rate limitations, the digital-domain processes can be preceded by a Track-and-Hold Amplifier (THA) and minimum analog-domain filtering as shown in Fig. 4 (b) and described in [22], to which the reader is referred. Here, we consider only the basic digital techniques. Note that other, more simplified, receiver structures are possible, that employ band-pass sampling of channels mapped into Nyquist Zones (NZs), and can "obtain" channels at pre-defined frequency locations (i.e. at predefined intermediate frequencies), as described in [22].

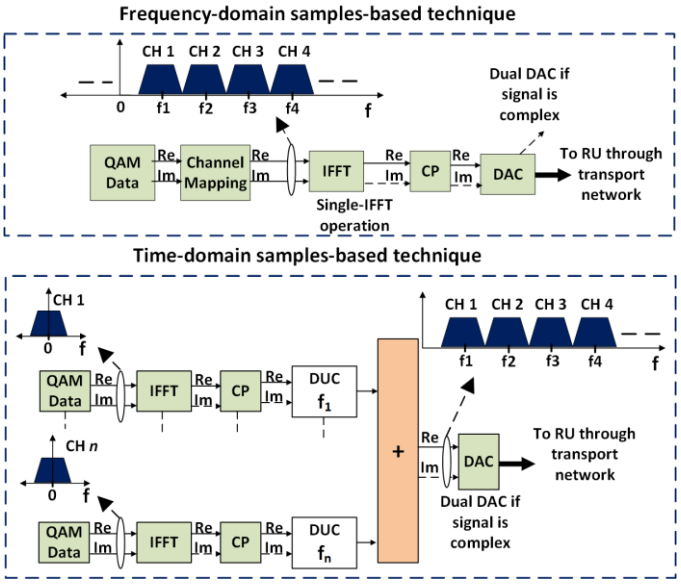

Fig. 3. Functional depiction of the two multiplexing techniques. Note that one numerology is shown here for simplicity, but in both cases, the processes within each technique can be scaled to generate channels comprising different numerologies. DAC, Digital-to-Analog Converter; QAM, Quadrature Amplitude Modulation; IFFT, Inverse-Fast Fourier Transform; CP, Cyclic Prefix; DUC, Digital Up-Converter;

3. COMPLEXITY ANALYSIS

In this section, the computation complexity of the two digital multiplexing techniques is considered. The analyses are general (i.e. not focused on particular use cases) and aimed at showing how computational complexity, given as the number of Multiplications Per Input Sample (MPIS), scales with multiplex parameters. Finally, sampling rates and computational latencies are examined.

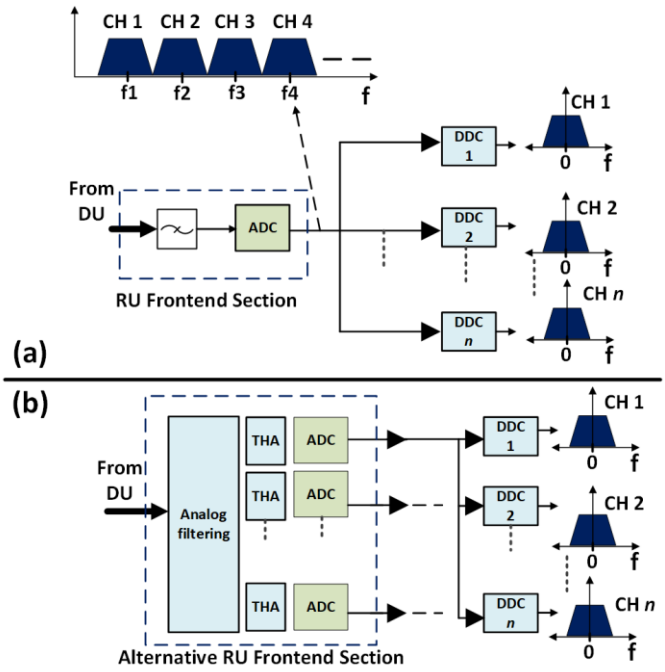

Fig. 4. Functional depiction of different de-multiplexing approaches: (a) Fully digital and (b) With minimal analog processing using a THA. THA, Track-and-Hold Amplifier; DDC, Digital Down-converter; ADC, Analog-to-Digital Converter.

A. Time-domain samples technique complexity

Time-domain processing complexity is principally determined by the DUC/DDC. The filtering/interpolation section of the DUC/DDC is a multi-stage implementation, consisting of a half-band filter, a Cascaded Integrator-Comb (CIC) compensator filter and a CIC interpolator as shown in Fig. 5. The only difference between the DUC and DDC is in the ordering of the filtering stages. Note, that this design represents a typical interpolation section in digital DUCs, although variations of this implementation are found (especially in the second stage filter, which is sometimes implemented as another half-band filter) [26], [27]. For the work presented here, all three filters are linear-phase Finite Impulse Response (FIR) implemented in a computationally efficient polyphase structure [28].

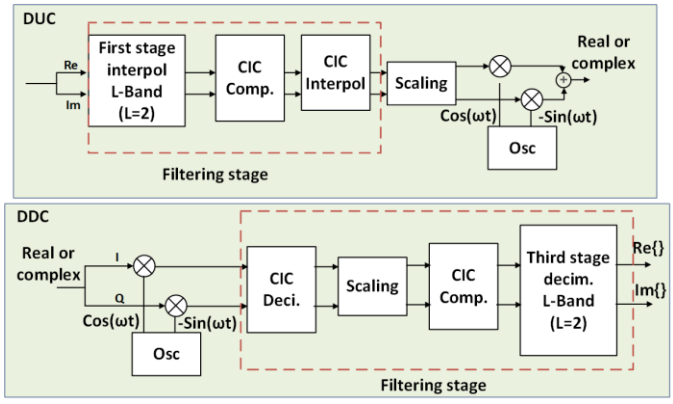

Fig. 5. The DUC (top) and DDC (bottom) processing stage.

Complexity results assume a minimum-order approach: the passband ripple and stopband attenuation are chosen, and the order of each filter (and, therefore, its complexity) is a consequence of these choices. Furthermore, only integer interpolation/decimation factors are assumed. Finally, a digital quadrature mixer, fed by a numerically controlled oscillator, is used to up-convert or down-convert the signal (in DUC or DDC, respectively). The filter structure uses the multi-rate algorithm available in MATLAB [29].

Fig. 6 shows the MPIS for the filtering stages of the DUC (or DDC) for different oversampling factors and stopband attenuations, assuming per-channel bandwidths of 100 MHz and 400 MHz. Note that for these results the interpolation factor is varied in accordance with the number of channels to be multiplexed, but the given MPIS values are for a single DUC (or DDC). Thus, the total MPIS value would require scaling of the values shown in Fig. 6 and Fig. 7 by the number of DUC/DDCs (which will be equal to the number of channels in the multiplex).

Complexity scales approximately linearly with oversampling factor. In general, the overall complexity is minimized by assigning most of the interpolation/decimation to the CIC interpolator/decimator stages, rather than the compensation stage. However, some choices of overall multiplication/division require assigning a higher value of interpolation/decimation to the intermediate compensation stage leading to deviations from the linear trend.

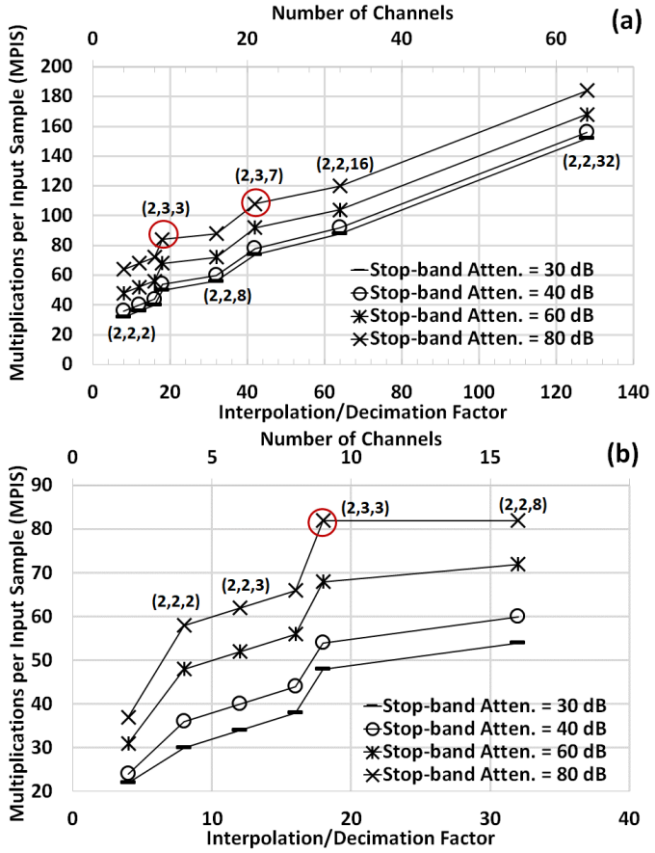

Fig. 6. Computational complexity, given as the number of multiplications per input sample (MPIS), of a single DUC/DDC stage for different oversampling factors and stopband attenuation factors, for a channel bandwidth (BW) of (a) 100 MHz and an IFFT size of 1024, and (b) 400 MHz and IFFT size of 4096. Interpolation factors for each filtering stages are shown as annotations.

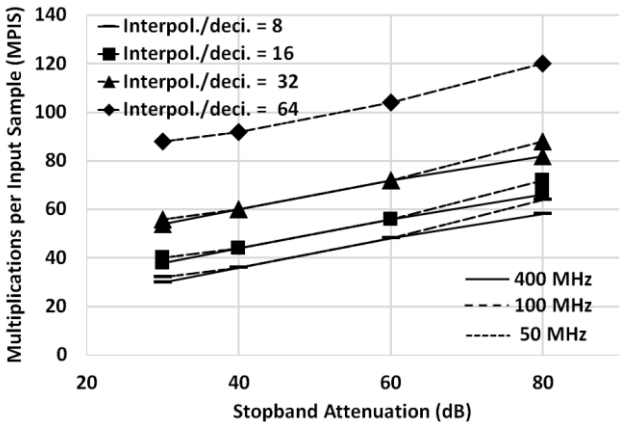

Fig. 7. Computational complexity, given as the number of multiplications per input sample (MPIS), of single DUC/DDC stage versus stop-band attenuation for different interpolation factors and channel bandwidths.

The complexity also scales approximately linearly with stopband attenuation, but is not generally affected by channel bandwidth, as can be seen in Fig. 7.

Note that for the highest interpolation/decimation factor (64), only the results for 50 MHz and 100 MHz bandwidths are considered. The traces corresponding to different bandwidths completely overlap for the 50 and 100 MHz results. A slight difference in MPIS for the highest bandwidth (400 MHz) is seen and that only for the highest (80 dB) and lowest (30 dB) stopband attenuations. Thus, it can be said that, overall, a change in channel bandwidth only leads to small variations in complexity for the different stopband attenuations.

B. Frequency-domain samples technique complexity

The MPIS for the technique based on frequency domain samples for the two different channel bandwidths are shown in Fig. 8. The MPIS scales logarithmically with number of channels, while larger bandwidths lead to increased complexity, as they require larger IFFT sizes. The assumed per-channel IFFT lengths are 1024 for 100 MHz bandwidth channels and 4096 for 400 MHz bandwidth channels.

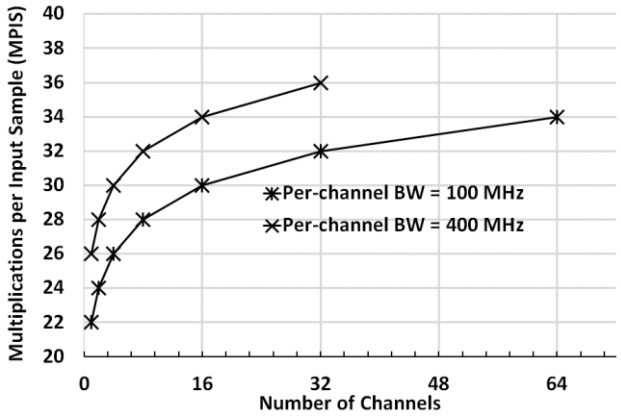

Fig. 8. Computational complexity, given as the number of computations per sample (MPIS), for different numbers of channels.

C. Combined complexity estimates for DU-RU

Fig, 9 shows a comparison of computational complexity in terms of MPIS, for the two techniques for 100 MHz and 400 MHz channel bandwidth, respectively, *including both transmitter and receiver processing*. For the time-domain samples technique, the complexity estimate includes the IFFT and a single DUC filtering stage at the DU and a single DDC at the RU. In other words, the total complexity for the time-domain samples technique would be the MPIS value scaled by the number of channels in the x-axis of Fig. 10. For the frequency-domain samples technique, it includes the single-IFFT at the DU and a single DDC at the RU. The frequency-domain samples technique clearly possesses lower overall complexity especially considering that the MPIS values for the time-domain samples technique are for a single DUC/DDC pair.

D. Sampling Rates

Fig. 10 shows a computation latency comparison for the two techniques for a per-channel bandwidth of 100 MHz. For the filtering stage of the DUC, and more so for increasing stop-band attenuation, there is an increase in group delay, measured in terms of the number of input samples that must be operated on for each output sample. The absence of the DUC and its filtering in the frequency domain samples technique leads to lower computation latency, whereas the small increase in latency with DUC processing for higher stop-band attenuations is a result of higher group delay in the filtering stages of the DUC.

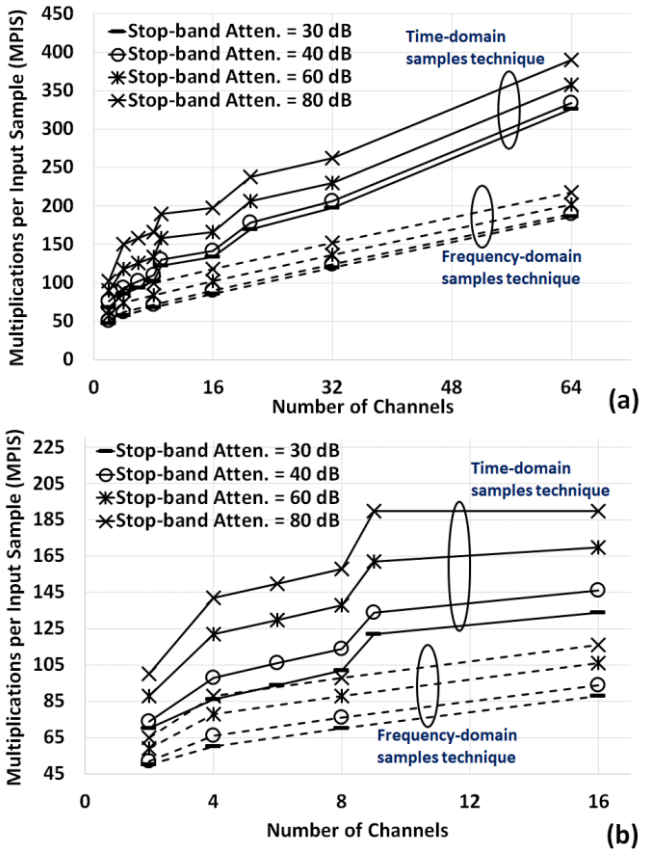

Fig. 9. Overall complexity comparisons for time-domain and frequency-domain samples techniques for a bandwidth of (a) 100 MHz. and (b) 400 MHz. Note that the complexity for the time-domain samples technique is for one IFFT/DUC/DDC stage only while for the frequency-domain samples technique it includes only one DDC stage.

The latency for both techniques is generally independent of the number of channels as an increase in the number of channels is

balanced by an appropriate increase in the sampling rate. The implied assumption is that samples are processed within the required sampling time; thus, the IFFT latency is simply the OFDM symbol duration. Therefore, these results offer an indication of the need to carry out less or more computations within the symbol duration. A latency comparison between DSP-assisted analog fronthaul and a digital fronthaul implementation is challenging due to processing being fundamentally implementation dependent. However, some estimates can be made with state-of-the art implementations. In [24], DSP implemented in a FPGA platform was used to select a channel within a band/multiplex of 6 wideband channels with a reported latency in the order of microseconds. In [20] a proof-of-concept experiment, comprising the transmission of 48 20-MHz LTE signals, reported a round-trip DSP latency of 2 microseconds. These reported values agree with the theoretical values in Fig. 10. In a digital fronthaul several aspects affect latency including mapping technique, number of aggregation points (e.g. Ethernet switching) and line rate. In [10] an overhead optimized mapper over a 10 GbE (Gigabit Ethernet) link resulted in a latency between 10 and 20 microseconds. However, this value only incudes the average packet generation latency at the DU. To transport the data required for even a single wideband RF channel a much large number of packets would have to be generated while at the RAU additional latency would result from processing these packets (de-framing, stop-and-wait buffering etc.).

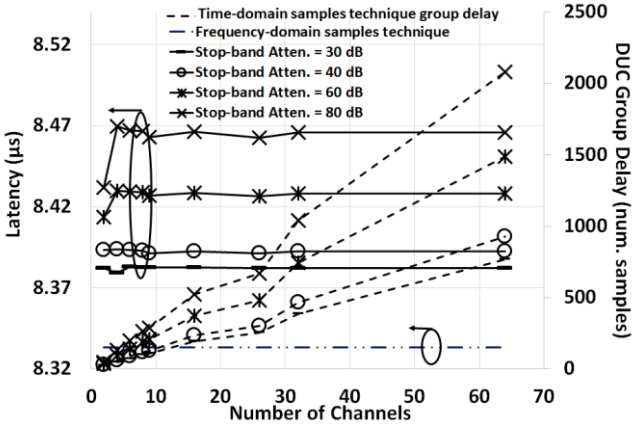

Fig. 10. Group delays for the DUC used in time-domain samples technique (right y-axis), and computation latency for time-domain and frequency-domain samples techniques (left y-axis) for 100 MHz per-channel bandwidth, for different stop-band attenuation.

There are significant differences in the sampling rate requirements of the two techniques. Fig. 11 shows required sampling rates for the two techniques, normalized to the per-channel sampling rate. Two cases are shown: in the first, the channel spacing is smaller than the bandwidth of the guard bands provided by null subcarriers in the IFFT of the channel; in the second case, the channel spacing is larger than this. In the cases studied the guard bands were approximately 25% of the channel bandwidth. While the time-domain samples technique has sampling rates that gracefully scale with the number of multiplexed channels, the frequency-domain samples technique, requires significant adjustments to accommodate non-power of 2 numbers of channels. Furthermore, for both techniques, some parameter adjustment needs to be made for larger channel spacing: either the DUC oversampling rate must be increased (time-domain samples technique) or the IFFT length must be increased to the next power-of-2 (frequency-domain samples technique). These step changes in sampling rate requirements for the frequency domain samples technique put it at a clear disadvantage for larger (larger than 25% of the channel bandwidth in this case) channel spacings and for multiplexes comprising non-power of 2 numbers of channels. Note, there is an implied assumption of powers-of-2 in the IFFT for the OFDM signals (as typically used in 3GPP standards). The possibility of using efficient non-powers-of-2 digital Fourier Transform processes is left for future investigation.

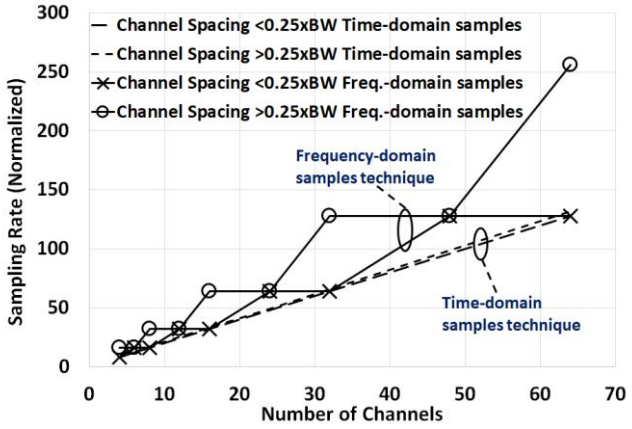

Fig. 11. DU sampling rates normalized by the per-channel sampling rate, for the frequency-domain and time-domain samples techniques.

4. MODELLING, SIMULATION AND PERFORMANCE ANALYSIS

A MATLAB-VPI (Virtual Photonics Inc) co-simulation environment was used in our assessment and is depicted in Fig. 12. VPI controls the simulation and calls the MATLAB transmitter processing functions, the outputs of which are passed as waveform samples to the VPI optical link model. At the receiver side, received sample streams from the VPI modelled link output are passed to MATLAB. Finally, performance estimates, such as EVM, of the de-multiplexed channels are performed in "run-time" in the MATLAB receiver code. The modeled, example optical link comprises a Mach-Zehnder Modulator (MZM) fed by a Continuous-Wave Laser (CWL). The optical signal at the output of the MZM is amplified by an Erbium Doped Fiber Amplifier (EDFA), transmitted over a short-length Single Mode Fiber (SMF) patch-cord, and received by a high-speed PIN-photodiode (PIN-PD).

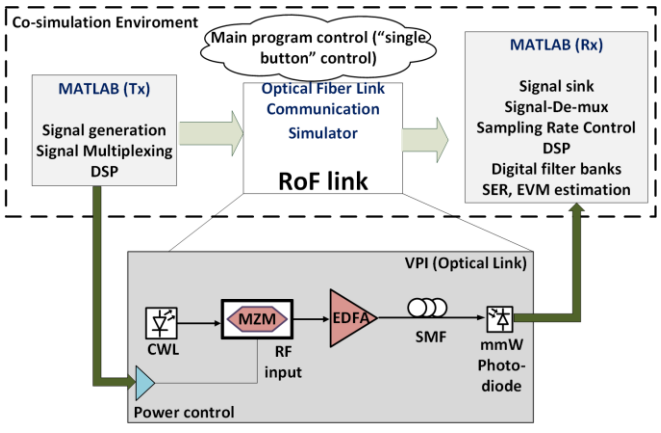

Fig. 12. Co-simulation environment and the modeled optical link. DSP, Digital Signal Processing; MZM, Mach-Zehnder Modulator; EDFA, Erbium Doped Fiber Amplifier; SMF, Single-Mode Fiber; CWL, Continuous-Wave Laser.

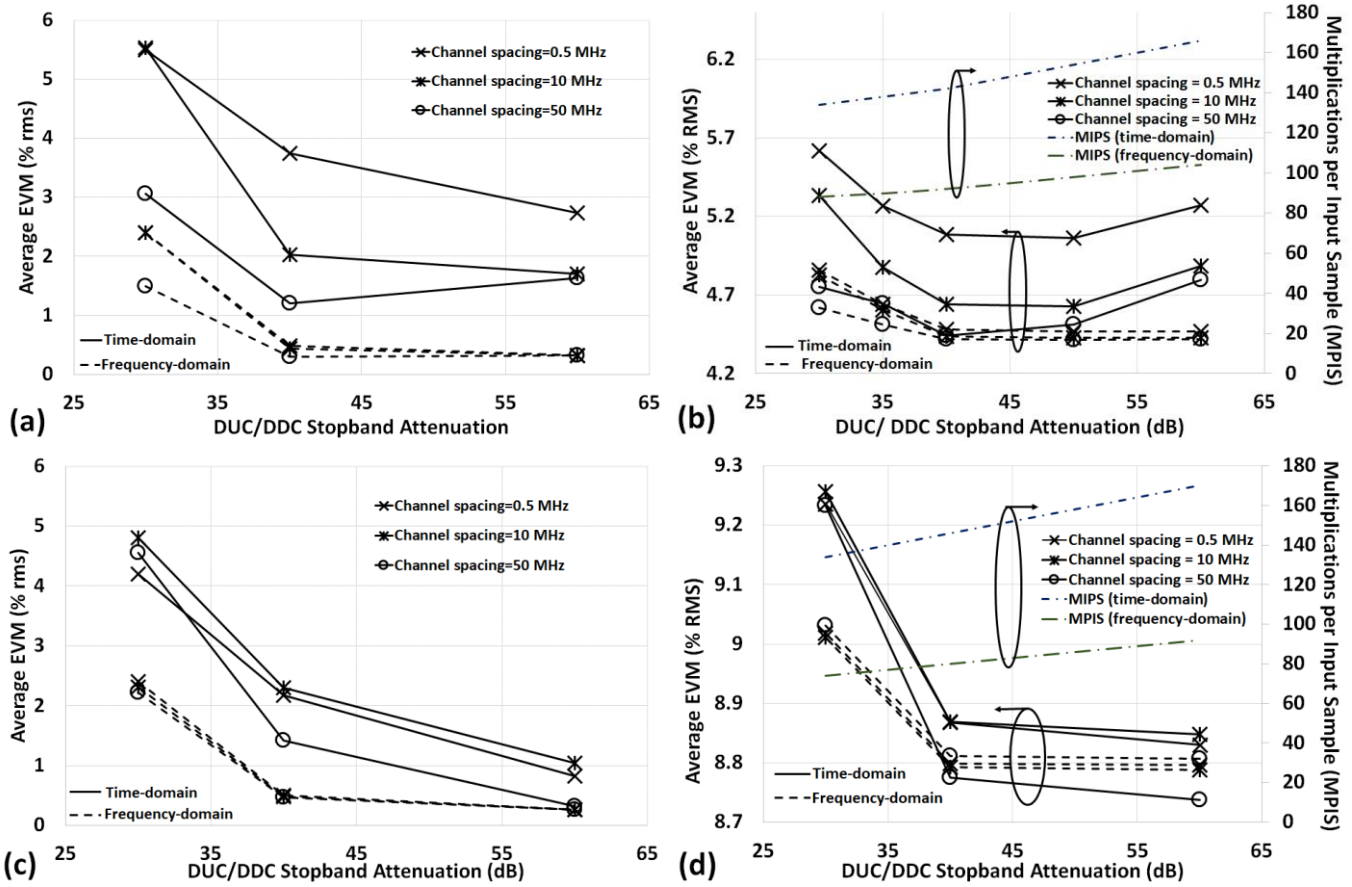

Fig. 13. Average EVM (% rms) results for time-domain samples and frequency-domain samples techniques for a multiplex comprising of 8 channels and an oversampling factor of 32 (of the per-channel bandwidth). (a) Baseline case (no optical link) for 100 MHz bandwidth channels. (b) Following transmission over the modeled RoF link and MPIS results for 100 MHz bandwidth channels. (c) Baseline case (no optical link) for 400 MHz bandwidth channels. (d) Following transmission over the modeled RoF link and MPIS results for 400 MHz bandwidth channels. Note that for the frequency-domain samples technique, the stopband attenuation is for the DDC at the receiver, while the MPIS results are for a single DUC/DDC.

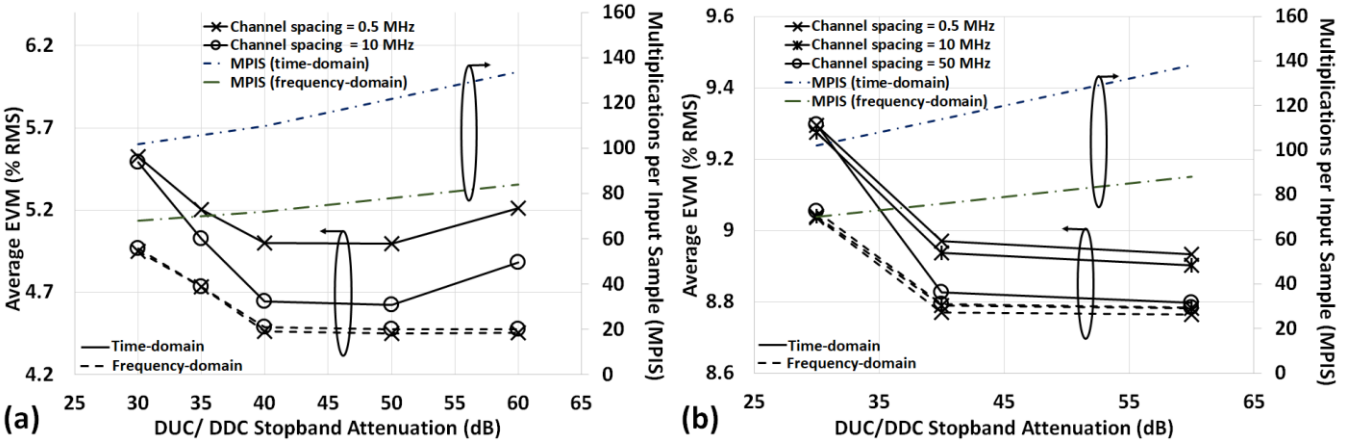

Fig. 14. Average EVM (% rms) and MPIS results for the time-domain samples and frequency-domain samples techniques following transmission over the modeled RoF link, for a multiplex comprising of 8 channels and an oversampling factor of 16 (of the per-channel bandwidth). (a) Per-channel bandwidth of 100 MHz. (b) Per-channel bandwidth of 400 MHz. Note that for the frequency-domain samples technique, the stopband attenuation is for the DDC at the receiver, while the MPIS results are for a single DUC/DDC.

The co-simulation environment and the matching of the optical link model to an experimental set-up has been described in [22] albeit in this work it is used with increased input optical powers from the CWL (10 dBm). The setup is used purely as an example to demonstrate implementation of the multiplexing techniques with a noisy, RoF link, that has been previously characterized, and should not be considered in itself to be a proposed fronthaul link.

As shown in Fig. 13, EVM is used to characterize performance, and results are reported for both a baseline case (no optical link) and for a case with the modeled optical link. In both cases the multiplex comprises of 8 channels, while an oversampling factor of 32 (of the per-channel sampling rate) is used.

The per-channel sampling rate is 122.88 MSps for the 100 MHz channels and 491.52 MSps for the 400 MHz ones. The 100 MHz channels comprise 832 data and 192 null subcarriers while for the 400 MHz channels these values are 3300 and 796, respectively. The modulation scheme in all cases is 16-QAM. The sampling rate used at the receiver is approximately 3.93 GHz and 15.7 GHz for the multiplex comprising of 100 MHz and 400 MHz channels, respectively. Note that while the sampling rate is high (especially for the multiplex comprising of 400 MHz channels) an arbitrarily lower sampling rate could be used with the receiver structure shown in Fig. 4 (b). The baseline case is used to establish EVM constraints that arise purely from the multiplexing/de-multiplexing process of each technique. The case with the optical link is used to show how much the multiplexing techniques might affect overall performance given the existence of noise and nonlinearities in real systems.

Generally, for the baseline case, the EVM performance improves significantly up to stopband attenuations of 40 dB, beyond which there is a lesser improvement, even a slight degradation in some cases. The effect of channel spacing is significant, due to reduced inter-channel interference with larger spacings. However, this effect is much less pronounced for the frequency-domain samples technique: it is less sensitive to channel spacing as a result of the generation process for the multiplex, which will always create channels that are orthogonal through its single IFFT operation. For this reason, the frequency-domain samples technique results in better EVM performance, but the difference in performance between the two techniques diminishes as the stopband attenuation is increased. With the optical link included, similar performance trends are observed although the difference between the techniques is somewhat obscured by the noise floor.

Fig. 14 shows EVM results for 100 MHz and 400 MHz channels for the case with the optical link, for a smaller oversampling factor of 16 (of the per-channel sampling rate). This factor is the minimum required to accommodate the 8 channels (and the frequency gaps in-between the channels). In this case, the sampling rate used at the receiver is approximately 2 GHz and 7.86 GHz for the multiplex comprising of 100 MHz and 400 MHz channels, respectively. Comparing these results with those for the case with the optical link in Fig 13, only minor performance degradation occurs as a result of the smaller oversampling factor, while the main behavioral trends that were observed in Fig. 13 are still present. Thus, an oversampling factor that results in a sampling rate equal to twice the two-sided bandwidth of the multiplex is adequate and no significant EVM performance gain is obtained with higher sampling rates. Note, however, that higher oversampling factors can have several benefits in practical implementations (they can aid time/frequency synchronization for example).

As a general confirmation of the performance trends observed in these results, an additional simulation was carried out for 16 100 MHz channels using the time-domain samples technique, the results of which are shown Fig. 15. In this case, the sampling rate used at the receiver is approximately 3.93 GHz. The trends remain for larger multiplexes, that is, the time-domain samples technique suffers with very narrow channel spacings, with improvement in performance occurring with larger stopband attenuations and/or larger channel spacings. Note that for the 50 MHz channel gap results, the sampling rate is somewhat higher to accommodate the larger channel spacing (larger than 25% of the channel bandwidth).

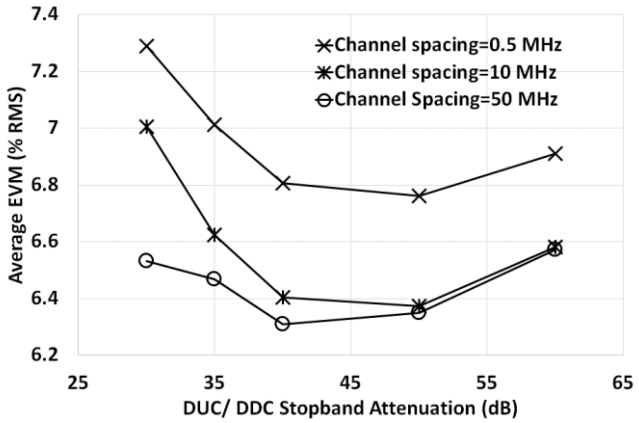

Fig. 15. Average EVM (% rms) results for time-domain samples technique and a multiplex comprising of 16 100 MHz channels and an oversampling factor of 32 (of the per-channel sampling rate).

Fig. 16 shows experimentally measured average EVM results for the two techniques, with a multiplex comprising of 8 100 MHz channels, following transmission over a short-span RoF link. In this case, the sampling rate used at the receiver is approximately 2 GHz. The measurement set-up is essentially as depicted in Fig. 12 but the optical link model (and its constituent components) are replaced by the real-world equivalents. The input multiplex is generated in MATLAB, as before, and is downloaded into an Arbitrary Waveform Generator (AWG). Following transmission over the RoF link, the received multiplex is captured by a fast oscilloscope for off line processing in MATLAB. More detailed information on the experimental set-up can be found in [22], where the same set-up was employed.

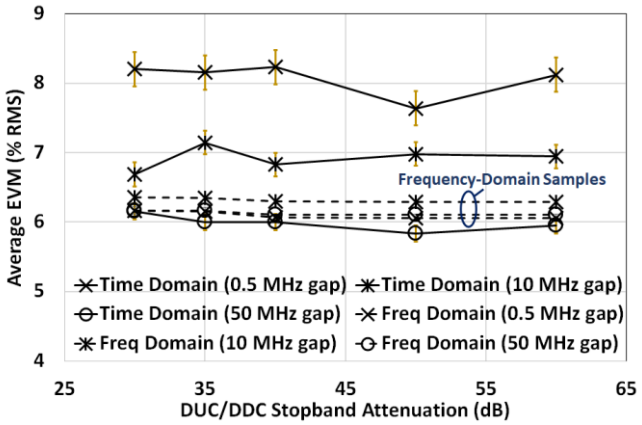

Fig. 16. Average EVM (% rms) for different channel spacings/gaps and DUC/DDC stopband attenuations, for the experimental results for the two multiplexing techniques and a multiplex comprising of 8 100 MHz channels and an oversampling factor of 16 (of the per-channel sampling rate).

Note that the results here are not directly comparable with those in Fig. 14 as the optical power available in the experimental set-up is

significantly lower (resulting in a higher noise floor) while the AWG only allows a set of predefined sample rates. Nevertheless, the results exhibit several of the trends observed in the simulation results (Figures 13 to 15). Namely, the time-domain approach suffers with narrow channel spacings but does show progressively improved performance as the channel spacing is increased. Furthermore, the standard deviation of the EVM, shown in the figure in the form of superimposed error bars, exhibits the same behavior: It is larger for the narrow channel spacings and becomes progressively smaller as the channel spacing is increased. On the other hand, the frequency-domain approach exhibits the trend of increased performance stability irrespective of channel spacing, while its standard deviation, even for the narrow channel spacing, is insignificant (it is included in the form of error bars but is not visible).

5. CONCLUSION

Two techniques for frequency-domain multiplexing, one directly processing/aggregating frequency-domain samples and the other time-domain samples, are thoroughly compared in terms of modulation quality performance, computational complexity, latency and sampling rate requirements. The frequency-domain samples technique is very flexible, and offers both lower overall complexity and better performance in terms of EVM. The time-domain approach is also flexible but requires significantly higher complexity and suffers with very narrow channel spacings, affecting the potential for achieving very high spectral efficiencies. However, under specific conditions, namely when transporting non-power of 2 numbers of channels and/or when employing larger channel spacings, the time-domain samples approach can lead to significantly reduced sampling rates and may thus be preferable.

Both techniques can be used in DSP-assisted analog fronthauling for 5G (and beyond) mobile networks offering a flexibility which is not achievable by traditional SCM methods, while combinations of the two techniques can be envisaged for a system that is even more flexible, and will thus be considered in a future article.

Funding sources and acknowledgments. Shabnam Noor and Philippos Assimakopoulos acknowledges support by the EU Horizon 2020 5G-DRIVE project.

Funding Information. EU Horizon 2020 5G-DRIVE project (grant agreement no. 814956)

References

1. Common Public Radio Interface (CPRI); Interface Specification, CPRI Specification V7.0, Oct. 2015 [Online]. Available: http://www.cpri.info/spec.html. Accessed on: Jan. 08, 2019.
2. T. Pfeiffer, "Next Generation Mobile Fronthaul and Midhaul Architectures [Invited]," IEEE/OSA J. of Opt. Comm. Netw., vol. 7, no. 11, pp. B38-B45, 2015.
3. P. Assimakopoulos, M. K, A-Hares, N. Gomes, "Switched Ethernet fronthaul architecture for cloud-radio access networks," IEEE/OSA J. of Opt. Comm. Netw., vol. 8, no. 12, pp. B135-B146, 2016.
4. Common Public Radio Interface: eCPRI Interface Specification, eCPRI Specification, V2.0, May 2019 [Online]. Available: http://www.cpri.info/spec.html. Accessed on: Jan. 08, 2019.
5. N. Gomes et al., "Boosting 5G Through Ethernet: How Evolved Fronthaul Can Take Next-Generation Mobile to the Next Level," IEEE Veh. Technol. Mag., vol. 13, no. 1, pp. 74-84, Mar. 2018.
6. Study on New Radio Access Technology: Radio Access Architecture and Interfaces (Release 14), 3GPP Technical Specification Group Radio Access Network, TR 38.801, V14.0.0, Mar. 2017 [Online]. Available: http://www.3gpp.org/DynaReport/38-series.htm. Accessed on: Jan. 08, 2019.
7. Release 15 Description; Summary of Rel-15 Work Items (Release 15), 3GPP Technical Specification Group Services and System Aspects, TR 21.915, V1.0.0, Mar. 2019 [Online]. Available: https://www.3gpp.org/DynaReport/status-report.htm. Accessed on: Apr. 08, 2019.
8. P. Sehier et al., "Transport evolution for the RAN of the future [Invited]," in IEEE/OSA J. of Opt. Comm. Netw., vol. 11, no. 4, pp. B97-B108, April 2019.
9. N. J. Gomes and P. Assimakopoulos, "Optical Fronthaul Options for Meeting 5G Requirements," in Proc. Int. Conf. on Transparent Optical Networks (ICTON), Bucharest, Romania, 2018, pp. 1-4.
10. P. Assimakopoulos et al., "A Converged Evolved Ethernet Fronthaul for the 5G Era," IEEE J. Sel. Areas Commun., vol. 36, no. 11, pp. 2528-2537, Nov. 2018.
11. ITU-T Series G, supplement 55, "Radio-over-fiber (RoF) technologies and their applications" 07/2015
12. ITU-T G.9803, "Radio over fibre systems", November 2018
13. Y. Yang, C. Lim and A. Nirmalathas, "Investigation on Transport Schemes for Efficient High-Frequency Broadband OFDM Transmission in Fibre-Wireless Links," J. Lightw. Technol., vol. 32, no. 2, pp. 267-274, Jan. 2014.
14. C. P. Liu and A. Seeds, "Transmission of Wireless MIMO-Type Signals Over a Single Optical Fiber Without WDM," IEEE Trans. Microw. Theory Tech., vol. 58, no. 11, pp. 3094-3102, 2010.
15. S. A. Khwandah, J. P. Cosmas, I. A. Glover, P. I. Lazaridis, N. R. Prasad and Z. D. Zaharis, "Direct and External Intensity Modulation in OFDM RoF Links," IEEE J. Photonics, vol. 7, no. 4, pp. 1-10, Jul. 2015.
16. C. Browning, A. Delmade, Y. Lin, D. Geuzebroek, and L. Barry, "Optical Heterodyne Millimeter-Wave Analog Radio-over-Fiber with Photonic Integrated Tunable Lasers," in Proc. Opt. Fiber Commun. Conf., (OFC), San Diego, CA, USA, 2019, paper W1I.4.
17. N. J. Gomes, P. Assimakopoulos, M. K. Al-Hares, U. Habib, S. Noor "The New Flexible Mobile Fronthaul: Digital or Analog, or Both?" in Proc. Int. Conf. on Transparent Optical Networks (ICTON), Trento, Italy, 2016, pp. 1-4.
18. C. Ranaweera, E. Wong, A. Nirmalathas, C. Jayasundara and C. Lim, "5G C-RAN with Optical Fronthaul: An Analysis from a Deployment Perspective," J. Lightw. Technol., vol. 36, no. 11, pp. 2059-2068, Dec. 2018.
19. M. Xu, J.-H. Yan, J. Zhang, F. Lu, J. Wang, L. Cheng, D. Guidotti and G.-K. Chang, "Bidirectional fiber-wireless access technology for 5G mobile spectral aggregation and cell densification," IEEE/OSA J. of Opt. Comm. Netw., vol. 8, no. 12, pp. 104-110, 2016.
20. X. Liu, H. Zeng, N. Chard, F. Effenberger, "Efficient Mobile Fronthaul via DSP-Based Channel Aggregation," J. Lightw. Technol., Vol. 34, No. 6, pp. 1556-1564, 2016.
21. M. Sung, S.-H. Cho, J. Kim, J. K. Lee, J. H. Lee and H. S. Chung, "Demonstration of IFoF-Based Mobile Fronthaul in 5G Prototype With 28-GHz Millimeter Wave," . Lightw. Technol., vol. 36, no. 2, pp. 601-609, Jan. 2018.
22. S. Noor, P. Assimakopoulos, N. J. Gomes, "A Flexible Subcarrier Multiplexing System with Analog Transport and Digital Processing for 5G (and beyond) Fronthaul," J. Lightw. Technol., vol. 37, no. 14, pp. 3689-3700, 15 Jul. 2019.
23. N. Argyris, et al., "A 5G mmWave Fiber-Wireless IFoF Analog Mobile Fronthaul link with up to 24 Gb/s Multi-band Wireless Capacity," J. Lightw. Technol, vol. 37, no. 12, pp. 2883-2891, Jun. 2019.
24. K. Tanaka et al., "First Experimental Demonstration of 5G Mobile Fronthaul Consisting of Cascaded IF-Over-Fiber Links, Frequency Converters and a Channel Selector," in Proc. European Conf. on Optical Commun. (ECOC), Rome, Italy, 2018, pp. 1-3.

25. C. Westphal, “Challenges in Networking to Support Augmented Reality and Virtual Reality (Invited)”, IEEE. Conf. on Computing, Networking and Communications (ICNC), Silicon Valley, CA, USA, 2017.
26. T. Tsou, Ettus Research Future Directions, 4th OAI Workshop, Paris, France, Nov. 2017 [Online]. Available: https://www.openairinterface.org/docs/workshop/4_OAI_Workshop_20171107/Talks/TSOU_oai-paris-ettus.pdf
27. National Instruments, *Building an Affordable 8x8 MIMO Testbed with NI USRP*, Apr. 2014.
28. N.J. Fliege, *Multirate Digital Signal Processing* , Wiley, 1994, pp. 229
29. Mathworks, *dsp.CICInterpolator system object* [Online]. Available: https://uk.mathworks.com/help/dsp/ref/dsp.cicinterpolator-system-object.html.